Optics Communications 392 (2017) 100–108

Contents lists available at ScienceDirect

Optics Communications

journal homepage: www.elsevier.com/locate/optcom

Speckle affected fringe detection based on three envelope extraction for self-mixing displacement measurement

Huang Zhen[a,*], Li Chengwei[b], Li Songquan[a], Zhang Zhenghe[a], Li Dongyu[a,*]

[a] School of Physics Science and Technology, Lingnan Normal University, Zhanjiang 524048, China
[b] School of Electrical Engineering and Automation, Harbin Institute of Technology, Harbin 150001, China

ARTICLE INFO

Keywords:
Self-mixing interference
Displacement measurement
Speckle effect
Envelope extraction

ABSTRACT

Speckle is an especially relevant issue as far as self-mixing interferometry works onto diffusive targets and for large displacements sensing. This article proposed a new signal processing technique, based on three envelope extraction transition detection algorithm, to correctly extract and processes self-mixing signals corrupted by speckle. The algorithm also discriminates the direction of the target movement for different self-mixing regimes. The validity of the proposed method was demonstrated by means of simulated signals and confirmed by several experimental measurements with envelope variation of a decade in amplitude. The use of this technique effectively removes the need for optical/electro-mechanical component and strict sampling number determination.

1. Introduction

Self-mixing interferometry (SMI) is nowadays an established instrumentation scheme notably for displacement measurement [1–3], due to its inherent simplicity, compactness and self-alignment, as well as the same fringe resolution as in traditional two beam interferometry [4]. As the self-mixing (SM) signal obtained may be noisy and different in the character of waveform, accurate signal processing is required for the optimum performance of SMI sensors and has been a source of constant activity, such as simple fringe counting [5], Fourier transform processing [6], the phase unwrap method (PUM) [7], Hilbert transform processing [8,9] and, more recently, the synthetic-wavelength SMI [10].

Speckle is an especially relevant issue as far as self-mixing interferometry works onto diffusive targets and for large displacements sensing. Donati et al. analyzed random errors occurring in SMI introduced by the speckle pattern [11]. In order to overcome the problem of amplitude fading by speckle, Norgia et al. proposed a bright-speckle tracking technique to look for high amplitude SM signal by scanning the target [12]. In a less mechanical context, Giuliani et al. used an electronic feedback loop as well as an optical arrangement to lock the system to half the interferometric fringe [13]. However, the external arrangements dismiss the fully integrated nature of this sensing technique. To relax this constraint, Norgia et al. added a liquid crystal attenuator to maintain moderate feedback regime, which is easier to exploit algorithmically [14]. However, its application range is limited, as not all surfaces can provide the necessary amount of backscattered light. Atashkhooei et al. applied a liquid lens to avoid signal fading via adaptively focal length variations. Despite the satisfactory impact of this modern component, the proposed method cannot be used at large speeds as the liquid lens has a slow time response [15]. They also proposed to use two LDs (LD, laser diode) with different wavelength and spot size pointing the same target to present different fading zones. The main disadvantages of this technique are that the measurement requires two SMI sensors, which need to be synchronized. Jha et al. demonstrated the use of the continuous wavelet transform to find the envelope of the SM signal and, thus, to keep track of speckle [16]. To avoid additional optical/electro-mechanical components, Zabit et al. proposed the use of a sliding window to determine the envelope of the SM signal and to locate the correct fringes for target reconstruction [17]. However an increase in either number of samples or rate of displacement can lead to omission of speckle modulated SM fringes. Arriaga et al. proposed a speckle-insensitive fringe detection method based on Hilbert transform [8]. However it is a similar phase observation.

In this paper, we demonstrate a simple and effective signal processing technique to correctly extract and process SM signals corrupted by speckle while maintaining its inherent simplicity, compactness and low the global cost of system. It is able to discriminate the direction of a remote target movement in the time domain, while lasers subject to different SM regimes, even for weak feedback with $C < 0.2$, without using heterodyne detection.

* Corresponding authors.
E-mail addresses: zzhuangzhen@163.com (H. Zhen), nanorainbows@163.com (L. Dongyu).

http://dx.doi.org/10.1016/j.optcom.2017.01.037
Received 23 September 2016; Received in revised form 21 January 2017; Accepted 23 January 2017
Available online 31 January 2017

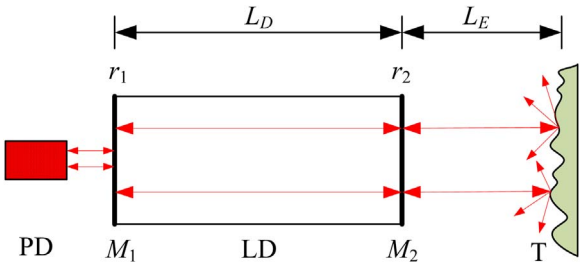

Fig. 1. Three mirror Fabry-Perot model of a laser cavity with optical feedback.

2. Self-mixing effect with speckle

SM effect occurs in a laser when a part of the beam backscattered by a remote target is coupled back into the laser cavity, interfering with the emitted beams and thus modifies the spectral properties of the laser. The self-mixing speckle interference was conventionally described by the well-known *Lang*-and-*Kobayashi* equations [2]. Here, we utilize the equivalent Fabry-Perot model to analyze it.

Fig. 1 introduces a three mirror Fabry-Perot model [2,18–20]. The length of laser cavity and external cavity are L_D and L_E. The refractive index of laser cavity and external cavity are n_c and n_T. The reflection coefficient of two facets of the LD, M_1 and M_2, are r_1 and r_2. The diffused surface is represented by T. When M_1 is defined to be the origin of coordinates in space, the electric field exited from M_1 can be written as

$$E = E_0 \exp[-i(\omega t + \varphi)] \tag{1}$$

where E_0, ω, φ are the amplitude, angular frequency and initial phase of the electric field, respectively.

The optical waves can be divided into two parts. One optical wave reflected by M_2 after one round-trip inside the laser cavity can be found as

$$E_1 = r_1 r_2 E_0 \exp[-i(\omega t + \varphi + 2n_c L_D k)] \tag{2}$$

where k is wave vector.

The other optical wave transmitted through M_2 is reflected by T and feedbacks into the laser cavity. When returning to M_1, this electric field can be written as

$$E_2 = E_0 \exp[-i(\omega t + \varphi + n_c L_D k + 2n_T k L_E)] \times \xi^2 U_0(x, y) \exp[-i\phi(x, y)] f \exp[-in_c L_D k] r_1 \tag{3}$$

where $U_0(x, y)$ and $\phi(x, y)$ are the change of amplitude and phase of the electric field which is generated by target surface roughness, x and y are coordinates in the coordinate planes of T, ξ is the coupling coefficient of the laser coupled from laser cavity to external cavity, f is the feedback ratio of external optical field coupled into laser cavity.

Two optical waves superpose on M_1. According to the threshold condition, when system is on steady state, the following equation can be obtained

$$r_1 f \xi^2 U_0(x, y) E_0 \exp\{-i[\omega t + \varphi + 2n_c L_D k + 2n_T k L_E + \phi(x, y)]\} + r_1 r_2 E_0 \exp[-i(\omega t + \varphi + 2n_c L_D k)] = E_0 \exp[-i(\omega t + \varphi)] \tag{4}$$

As the refractive index of laser cavity can be expressed as: $n_c = n + ig$, where g is the threshold gain [18], the following equation can be obtained

$$r_1 r_2 \exp(2gL_D k) \exp(-i \cdot 2nL_D k) \cdot \left\{1 + \frac{r_1 f \xi^2 U_0(x, y)}{r_2} \exp\{-i[2n_T k L_E + \phi(x, y)]\}\right\} = 1 \tag{5}$$

By rearranging Eq. (5), it can be expressed as

$$r_1 r_2 \exp(2gL_D k) \exp(-i \cdot 2nL_D k) \exp[-i\theta(x, y)] \cdot \sqrt{\{1 + \beta(x, y)\cos[2n_T k L_E + \phi(x, y)]\}^2 + \{\beta(x, y)\sin[2n_T k L_E + \phi(x, y)]\}^2} = 1 \tag{6}$$

where $\beta(x, y) = \xi^2 f U_0(x, y)/r_2$ and $\theta(x, y) = \arctan\frac{\beta(x, y)\sin[2n_T k L_E + \phi(x, y)]}{1 + \beta(x, y)\cos[2n_T k L_E + \phi(x, y)]}$.

While $\beta(x, y) \ll 1$,

$$\theta(x, y) \approx \beta(x, y)\sin[2n_T k L_E + \phi(x, y)] \tag{7}$$

$$\sqrt{\{1 + \beta(x, y)\cos[2n_T k L_E + \phi(x, y)]\}^2 + \{\beta(x, y)\sin[2n_T k L_E + \phi(x, y)]\}^2} \approx 1 + \beta(x, y)\cos[2n_T k L_E + \phi(x, y)] \tag{8}$$

Substituting Eqs. (7) and (8) into Eq. (6), we can obtain

$$r_1 r_2 \exp(2gL_D k)\{1 + \beta(x, y)\cos[2n_T k L_E + \phi(x, y)]\} \exp\{-i \cdot [2knL_D + \beta(x, y)\sin(2n_T k L_E + \phi(x, y))]\} = 1 \tag{9}$$

From Eq. (9), we can obtain

$$2knL_D + \beta(x, y)\sin[2n_T k L_E + \phi(x, y)] = 2M\pi \tag{10}$$

$$gk = -\frac{1}{2L_D}\{\ln|r_1 r_2| + [\beta(x, y)\cos(2n_T k L_E + \phi(x, y))]\} \tag{11}$$

As n and g can be expressed as $n = n_0 + \chi\Delta N$, $g = g(x,y) = g_0 + \rho\Delta N(x,y)$, where n_0 and g_0 are the real and imaginary part of n_c without target, respectively, ΔN is the change of the carrier density, χ and ρ are the rate of change of the real and imaginary part of n_c with the change of the carrier density. And $k = k_0 + \Delta k$, k_0 is the corresponding vacuum wave vector modulus without optical feedback, Δk is the change of the wave vector modulus [18]. Substituting them into Eqs. (10) and (11)

$$2(k_0 + \Delta k)(n_0 + \chi\Delta N)L_D + \beta(x, y)\sin[2n_T k L_E + \phi(x, y)] = 2M\pi \tag{12}$$

$$(g_0 + \rho\Delta N)(k_0 + \Delta k) = -\frac{1}{2L_D}\{\ln|r_1 r_2| + [\beta(x, y)\cos(2n_T k L_E + \phi(x, y))]\} \tag{13}$$

Without optical feedback, Eq. (11) can be expressed as

$$g_0 k_0 = -\frac{1}{2L_D}\ln|r_1 r_2| \tag{14}$$

Treating ΔN and $\Delta\omega = c\Delta k$ as independent variables and dropping $\Delta N\Delta\omega$ crossterms, where c is the speed of light in vacuum. We obtain from Eqs. (12–14)

$$\omega\tau - \omega_0\tau = -C\sin\{[\omega\tau + \phi(x, y)] - \arctan(\alpha)\} \tag{15}$$

$$\Delta G(x, y) = gk - g_0 k_0 = -\frac{\beta(x, y)}{2L_D}\cos[\omega\tau + \phi(x, y)] \tag{16}$$

where $\omega_0 = ck_0$ and $\omega = ck$, are angular frequency of the electric field without and with optical feedback, respectively, $\tau = 2n_T L_E/c$, $\omega\tau = 2n_T k L_E$, $\alpha = \chi/\rho$ is the linewidth enhancement factor, and C is the feedback factor.

$$C = \frac{c\beta(x, y)\sqrt{1 + \alpha^2}}{2nL_D(1 + g_0\alpha/n_0)} \tag{17}$$

For target with a displacement of $D(t)$ and let $n_T = 1$, the output power variation of the LD can be known as

$$P_s(t) = -\frac{\beta(x, y)}{2L_D}\cos\left[\frac{4\pi L_E(t)}{\lambda_F(t)} + \phi(x, y)\right] \tag{18}$$

where $L_E(t) = L_0 + D(t)$, L_0 is the initial distance between laser and target, $D(t)$ is the target displacement and $\lambda_F(t) = 2\pi/k$ is the emission wavelength subject to feedback.

A random rough surface with Gaussian statistics is generated using a method outlined by Garcia and Stoll [21], where an uncorrelated distribution of surface points using white noise is convolved with a Gaussian filter to achieve correlation. In this paper, we use the Matlab codes developed by Dr. David Bergström to generate rough surface [22]. The simulation parameters are number of surface points (N=1e4), length of surface side (rL=25 μm), root mean square height (r=0.5 μm), correlation length in x (clx=5 μm), and correlation length in y (cly=5 μm). The random rough surface is shown in Fig. 2(a), its

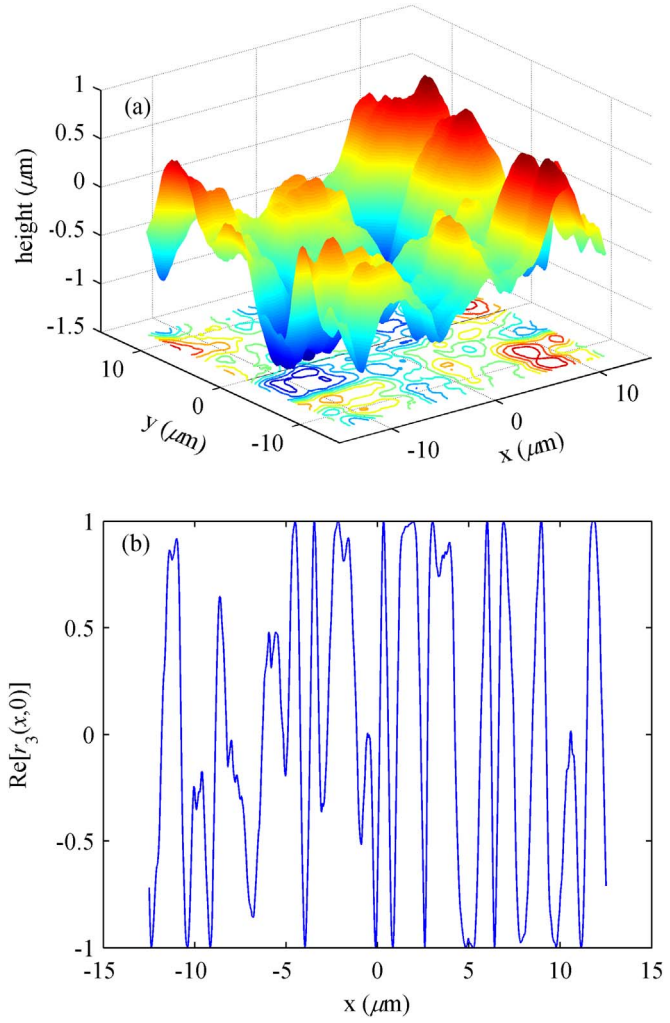

Fig. 2. (a) A random rough surface with average roughness value of 0.27 m and (b) the spatial variation of Re[$r_3(x,0)$].

average roughness value (Ra) is 0.27 μm, and the spatial variation of the real part of target reflection coefficient, expressed as Re[$r_3(x,y)$], is shown in Fig. 2(b).

The target is initially placed at 10 mm from the LD and moved away from the laser with a displacement of 0.25 mm. The wavelength used in simulations is 650 nm. Fig. 3(b) shows the speckle affected SM signal obtained, expressed as $P_s(t)$. The C values presented in Fig. 3(a) are calculated by Eq. (17). The depth of speckle-induced modulation is about 4.65. And the depth of speckle-induced modulation is defined as the ratio of amplitude of the envelope corresponding to the biggest detected SM fringe to the amplitude of the envelope corresponding to the smallest detected SM fringe [17]. As shown in Fig. 3(b), very relevant changes in amplitude appear during the target movement which making very complex to properly recognize the transitions. And variations in C can strongly influence the waveform of SM signals. In fact, variations in C cause changes in the SM feedback regimes varying from weak to moderate to strong feedback, where each regime would require specific signal processing for displacement reconstruction [17]. It may also bring on relevant inaccuracies in displacement reconstruction procedures. Especially for $C < 0.2$, it is hard to identify the direction of target from SM signal directly, because the SM signal fringes are almost sinusoidal [23].

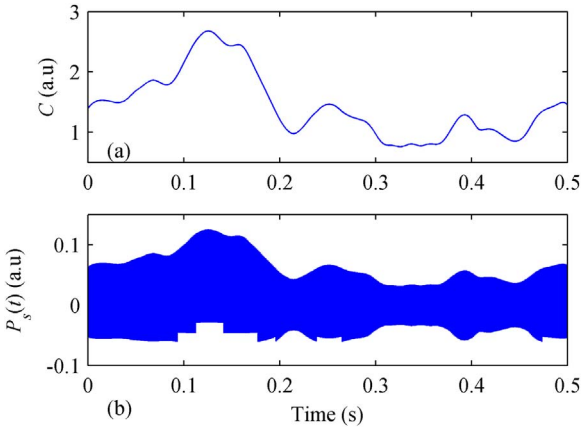

Fig. 3. (a) The corresponding C values and (b) a SM signal with speckle.

3. Principle of three envelope extraction transition detection algorithm

For a typical SM signal that is not affected by speckle, SM fringes can be easily detected by using the fixed/adaptive threshold values [23,24]. And then displacement can be reconstructed with a resolution of $\lambda/2$ by using simple fringe counting, or better resolution by PUM. All of these methods are based on the normalized and zero-crossing SM signal. In order to extract a normalized and zero-crossing signal from speckle affected signal and to detect transitions correctly from the normalized and zero-crossing SM signal with different C, the transition detection algorithm based on three envelope extraction is illustrated in Fig. 4. The signal processing algorithm consists of the following principal steps.

3.1. Filtering

First of all, the speckle affected SM signal $P_s(t)$ is filtered by using a low pass filter to eliminate high frequency noise present in the SM signal. Fig. 5 presents a segment of a SM signal before and after the filtering. It thus allows a better extraction of the envelopes of the corresponding signals later.

3.2. Envelope extraction #1 for a zero-crossing SM signal

In order to obtain a zero-crossing SM signal, the upper and lower envelopes of the filtered SM signal $P_{sf}(t)$ are recovered by using a local maximum detection and a local minimum detection. The median of $P_{sf}(t)$, $median(t)$, is obtained by Eq. (19). And then a zero-crossing SM signal $P_z(t)$ is got by Eq. (20).

$$median(t) = env_{max}(t) - [env_{max}(t) - env_{min}(t)]/2 \quad (19)$$

$$P_z(t) = P_{sf}(t) - median(t) \quad (20)$$

where $env_{max}(t)$ and $env_{min}(t)$ are the local maximum and local minimum of $P_{sf}(t)$, respectively.

The upper and lower envelopes of $P_{sf}(t)$ are indicated in Fig. 6(a) in red and in green, respectively. And the obtained zero-crossing SM signal $P_z(t)$ is shown in Fig. 6(b).

3.3. Envelope extraction #2 for a normalized SM signal

In order to get a normalized SM signal from the zero-crossing SM signal, the upper envelope of the obtained zero-crossing SM signal is recovered by using the local maximum detection again, expressed as $env_{\max 1}(t)$. And then the normalized and zero-crossing SM signal $P(t)$ is retrieved by Eq. (21).

$$P(t) = P_z(t)/env_{\max 1}(t) \quad (21)$$

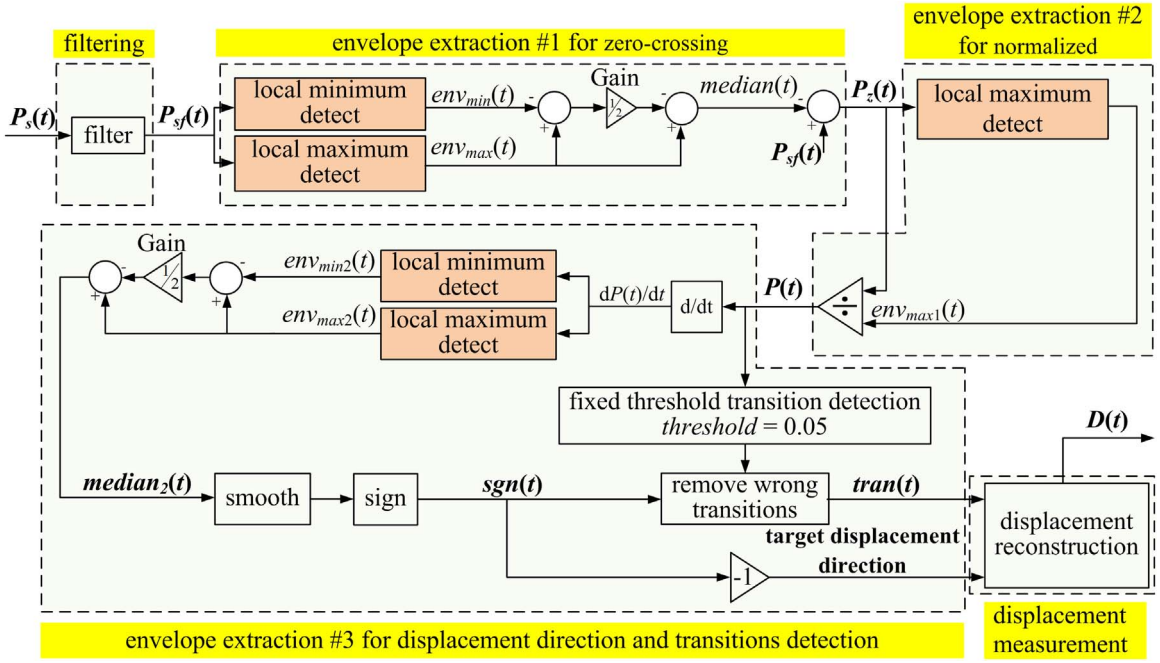

Fig. 4. Three envelope extraction transition detection algorithm.

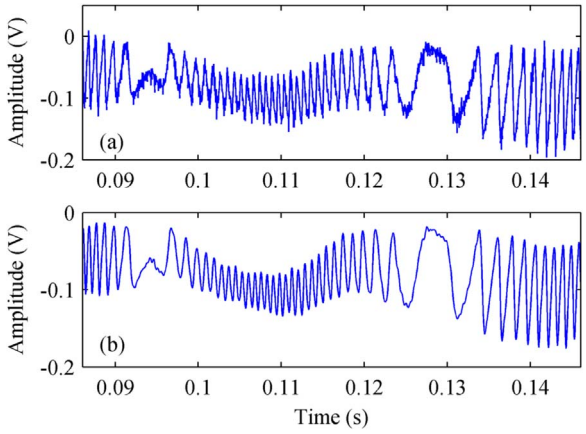

Fig. 5. (a and b) A segment of SM signal before and after low pass filtering.

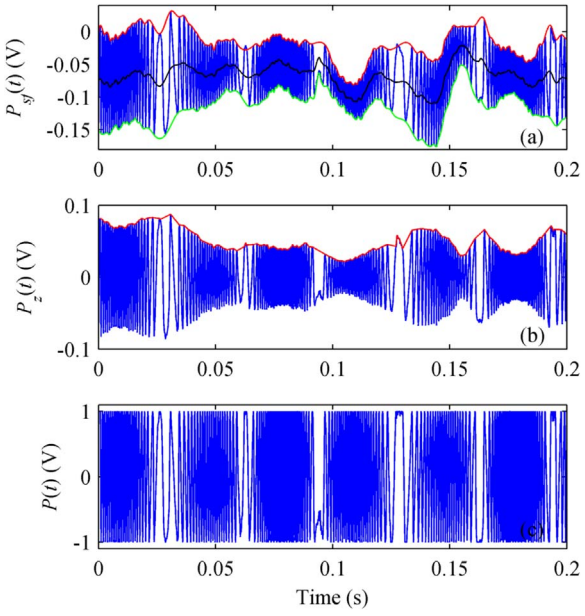

Fig. 6. (a) $P_{sf}(t)$ in blue, its upper envelope (in red), its lower envelope (in green), and $median(t)$ (in black), (b) $P_z(t)$ in blue and its upper envelope (in red), and (c) $P(t)$. (For interpretation of the references to color in this figure legend, the reader is referred to the web version of this article.)

Fig. 6(c) presents the normalized and zero-crossing SM signal retrieved from the speckle affected SM signal shown in Fig. 6(a).

3.4. Envelope extraction #3 for displacement direction and transitions detection

Usually, the derivative of the arccos($P(t)$) is then compared with a threshold value (or an adaptive threshold value) to ascertain the presence of a transition (or a fringe) through a transition detector. However, these methods can only be applied to the SM signal with a constant optical feedback factor C in the whole section.

Let's consider the standard simulation SM signal first. Fig. 7 shows four SM signals for a sinusoidal displacement with C=0.001, 0.5, 1, and 3, respectively. The corresponding signals of $dP(t)/dt$ are shown in Fig. 8, and their upper and lower envelopes, expressed as $env_{max2}(t)$ and $env_{min2}(t)$, are detected and marked in red and green, respectively. It's shown that the difference between the amplitude of the upper and lower envelope increases with the increasing of C. According to Eq. (22), the medians of $dP(t)/dt$, expressed as $median_2(t)$, are shown in Fig. 8 and Fig. 9 in black. It's noted that the median of $dP(t)/dt$ while C=0.001 is very small. In order to show it clear in one graph with other curves, it's magnified 25 times. The red lines shown in Fig. 9 are the sign of $median_2(t)$, expressed as $sgn(t)$.

$$median_2(t) = env_{max2}(t) - [env_{max2}(t) - env_{min2}(t)]/2 \quad (22)$$

Compared with target displacement shown in Fig. 7(a), it's worth noting that the sign of $median_2(t)$ is opposite to the direction of the target displacement. The direction of the target displacement can be identified by the sign of $median_2(t)$ directly. $sgn(t)$=−1 and 1 represent the target displacement away and towards the LD respectively. Therefore, the direction of the target displacement is obtained by $(-1)\cdot sgn(t)$.

Fig. 9 shows the transitions detected by a threshold of 0.05. As reported in Ref. [23], in case of $1 < C < 4.6$, transitions can be correctly detected by a relatively small threshold(Fig. 10(d)); in case of $0.2 < C <$

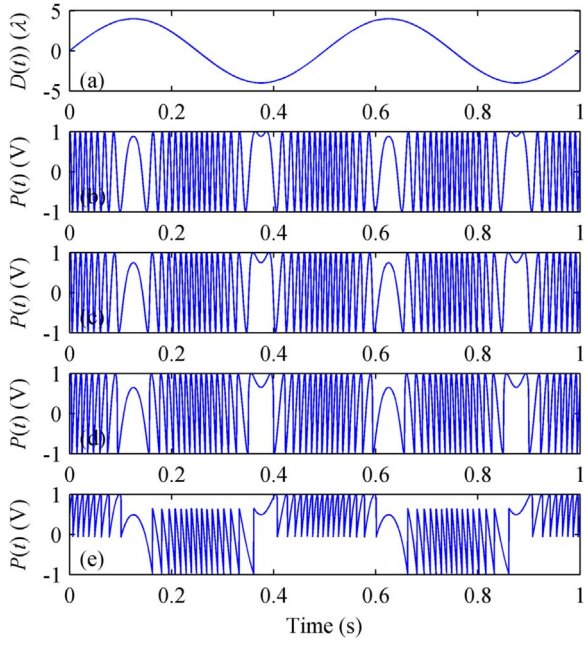

Fig. 7. (a) $D(t)$ and $P(t)$ with C=0.001 (b), C=0.5 (c), C=1 (d) and C=3 (e).

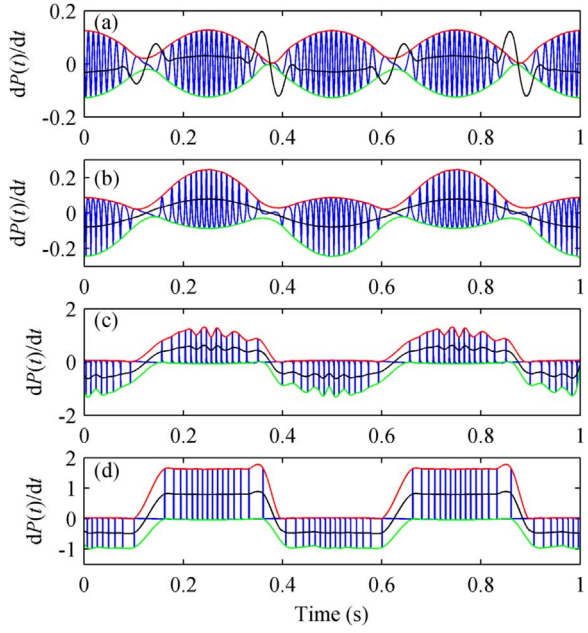

Fig. 8. d$P(t)$/dt (in blue), its upper envelope (in red), its lower envelope (in green) and $median_2(t)$ (in black) with C=0.001 (a), C=0.5 (b), C=1.5 (c) and C=3 (d). (For interpretation of the references to color in this figure legend, the reader is referred to the web version of this article.)

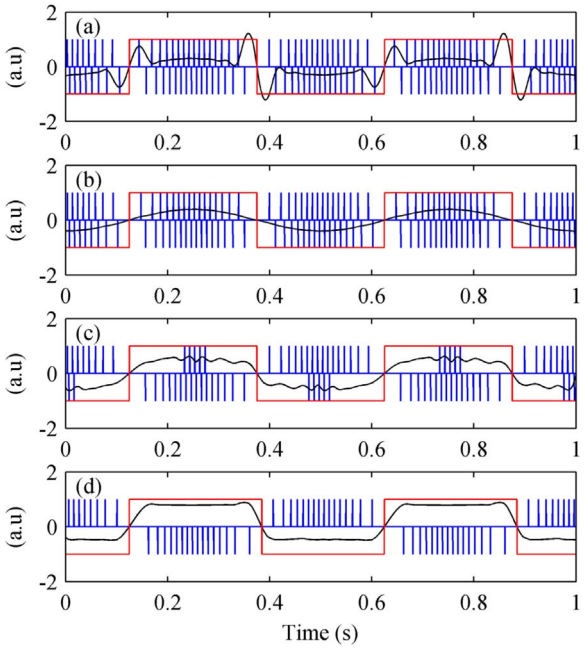

Fig. 9. Transitions with threshold =0.05 (in blue), $median_2(t)$ (in black) and $sgn(t)$ (in red) with C=0.001 (a), C=0.5 (b), C=1.5 (c) and C=3 (d). (For interpretation of the references to color in this figure legend, the reader is referred to the web version of this article.)

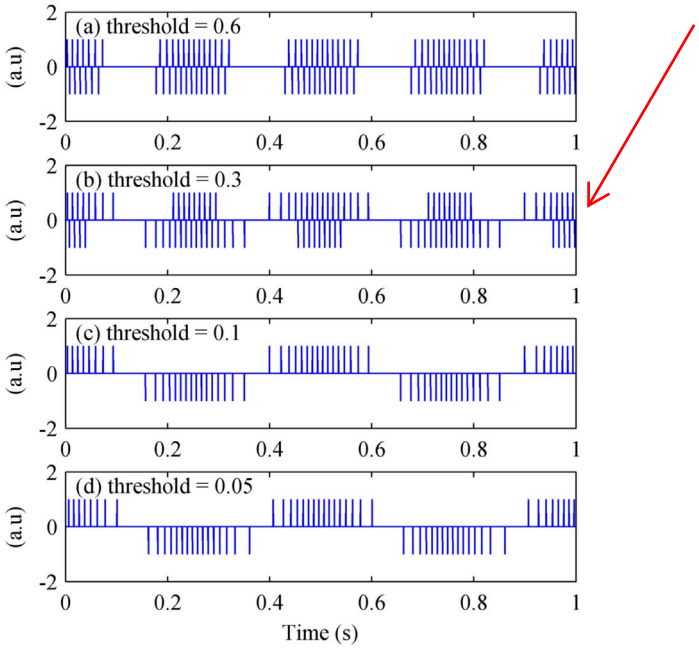

Fig. 10. Transitions with C=0.001 (a), C=0.5 (b), C =1.5 (c) and C=3 (d).

1, the more the value of C approaches 0.2, the more the shape of SM fringes loses its sawtooth aspect and tends to be sinusoidal, therefore it needs a relatively large threshold to correctly detect the transitions(Fig. 10(b) and (c)); and in case of $0 < C < 0.2$ where the SM signal fringes are almost sinusoidal in shape thus resulting in equal number of positive and negative transitions within a region(Fig. 10(a)), it's not able to correctly detect the transitions directly by increasing the value of the threshold.

In order to extract correct transitions, transitions are selected by judging the sign of themselves according to the sign of $median_2(t)$. Only the positive transitions should be obtained while $sgn(t) < 0$, and only negative transitions should be obtained for the SM signal corresponding to $sgn(t) > 0$. Fig. 11 shows the corresponding correct transitions.

However, noise interference is inevitable. It will impact the accuracy of envelope extraction, and then affect the correct extraction of the median of d$P(t)$/dt. Therefore an average filter is used to smooth $median_2(t)$. Fig. 12(b) and (c) shows the transitions of SM signal shown in Fig. 6(a) before and after smoothing.

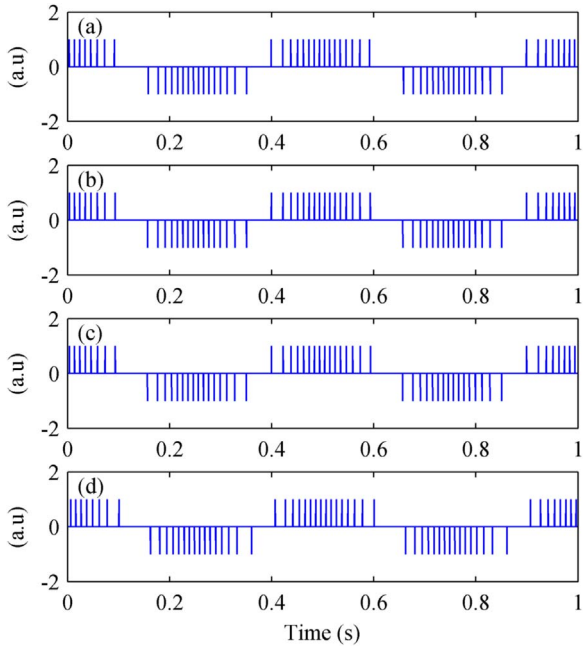

Fig. 11. Correct transitions with C=0.001 (a), C=0.5 (b), C=1.5 (c) and C=3 (d).

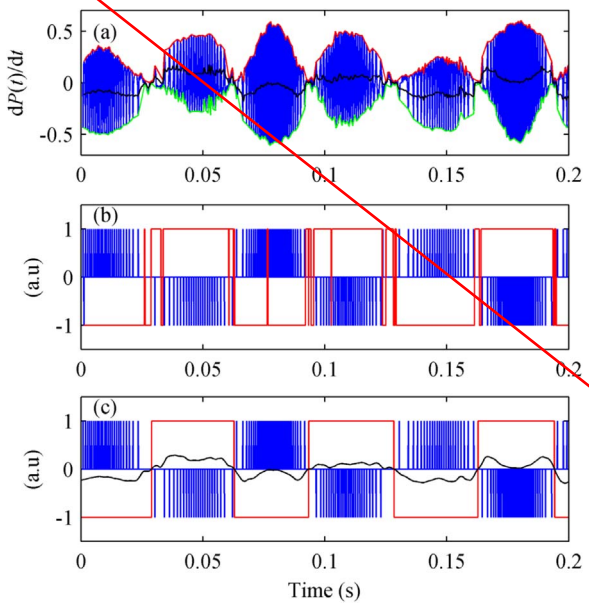

Fig. 12. (a) d$P(t)$/dt (in blue), its upper envelope (in red), its lower envelope (in green), and $median_2(t)$ (in black), (b) transitions (in blue) and $sgn(t)$ (in red) before smoothing and (c) transitions (in blue), $2{\cdot}median_2(t)$ (in black) and $sgn(t)$ (in red) after smoothing. (For interpretation of the references to color in this figure legend, the reader is referred to the web version of this article.)

3.5. Displacement measurement

After correct detection of transitions, displacement can then be recovered by fringe counting method providing $\lambda/2$ resolution and other displacement reconstructed methods. As shown in Fig. 13, the speckle-induced modulation of this signal is about 4.3. The normalized and zero-crossing SM signal obtained by the proposed technique is shown in Fig. 13(b). The reconstructed displacement by fringe counting method, expressed as $D_{\lambda/2}(t)$, is represented in Fig. 13(c) in red, and the corresponding maximum error is about 258 nm for maximum displacement amplitude of 13.7 μm.

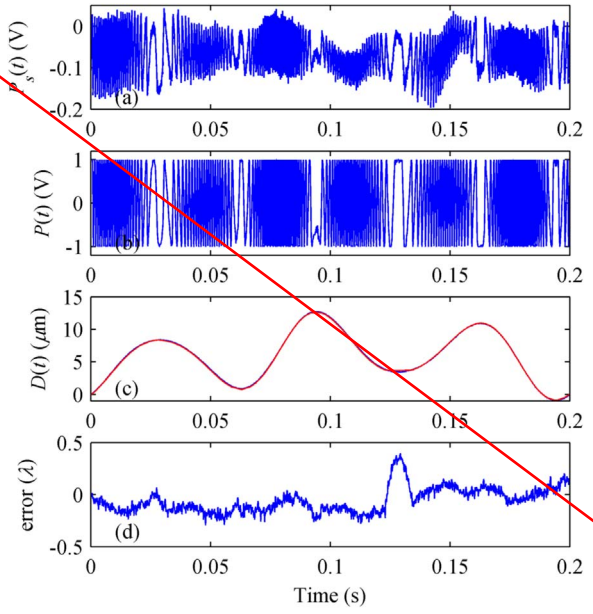

Fig. 13. Displacement reconstructed results for an aleatory displacement: (a) $P_s(t)$, (b) $P(t)$, (c) $D_{\lambda/2}(t)$ (in red) and reference displacement (in blue) and (d) error. (For interpretation of the references to color in this figure legend, the reader is referred to the web version of this article.)

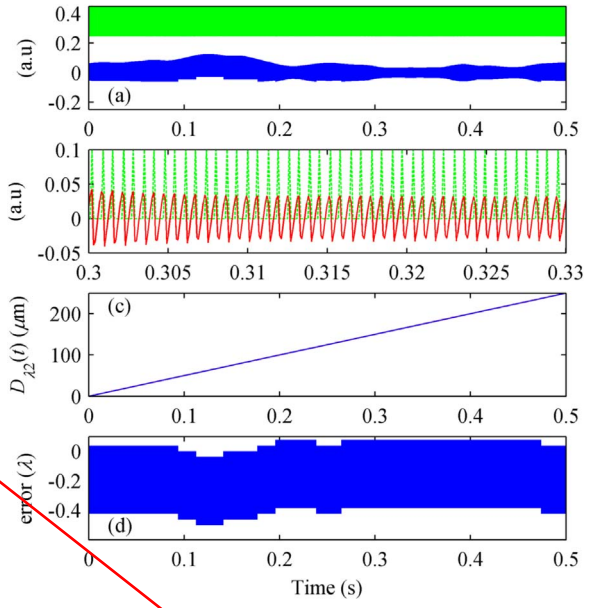

Fig. 14. Displacement reconstructed results for a large displacement: (a) $P_s(t)$ (in blue) and transitions (in dotted green), (b) Zoom on the deeply modulated fringes (in red) and the corresponding transitions (in dotted green), (c) displacement reconstructed by fringe counting $D_{\lambda/2}(t)$ and (d) error. (For interpretation of the references to color in this figure legend, the reader is referred to the web version of this article.)

4. Simulation results

The proposed three envelope extraction transition detection algorithm has been tested on several simulations. Fig. 14(a) shows the transitions detection results of the speckle affected SM signal for a large displacement shown in Fig. 3(b). All of SM transitions are correctly detected, and transitions of the deeply modulated fringes are shown in Fig. 14(b), where each fringe has been individually tracked. Displacement reconstructed by fringe counting method is shown in Fig. 14(c). The maximum error is less than $\lambda/2$.

Fig. 15(c) shows a simulated speckle affected SM signal of an aleatory displacement with the maximum displacement amplitude of

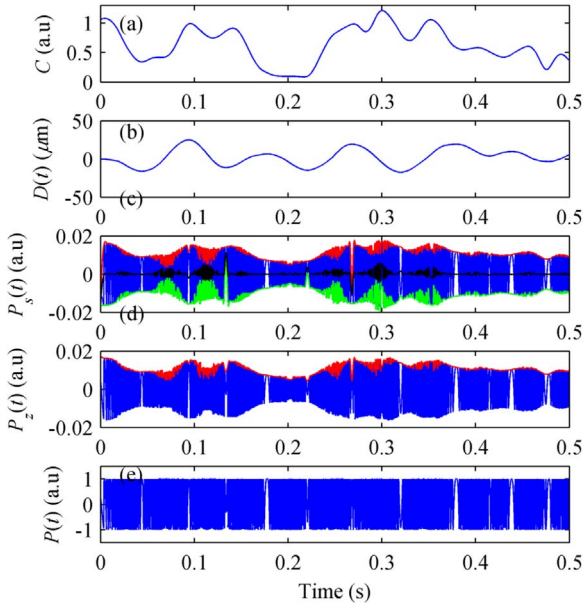

Fig. 15. (a) C, (b) $D(t)$, (c) $P_s(t)$ (in blue), its upper envelope (in red), its lower envelope (in green) and $median(t)$ (in black), (d) $P_z(t)$ (in blue) and its upper envelope (in red) and (e) $P(t)$. (For interpretation of the references to color in this figure legend, the reader is referred to the web version of this article.)

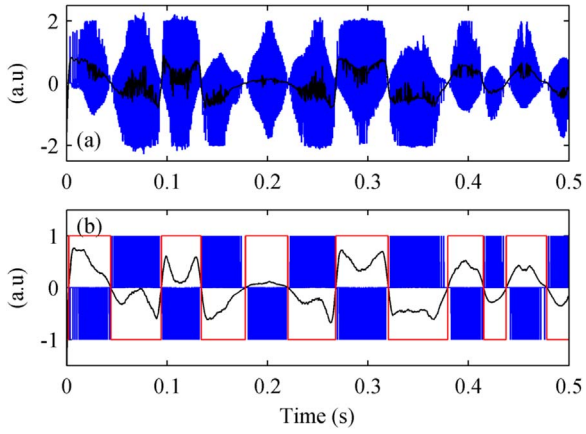

Fig. 16. (a) $dP(t)/dt$ (in blue) and $median_2(t)$ before smoothing (in black) and (b) transitions (in blue), $median_2(t)$ after smoothing (in black) and $sgn(t)$ of the $median_2(t)$ after smoothing (in red). (For interpretation of the references to color in this figure legend, the reader is referred to the web version of this article.)

25 μm. The depth of speckle-induced modulation is about 4.40. The corresponding C and displacement are shown in Fig. 15(a) and (b), respectively. After the processing of the envelope extraction #1 and #2, the signals of $P_z(t)$ and $P(t)$ extracted are shown in Fig. 15(c) and (d), respectively. And after the processing of envelope extraction #3, the signal of $dP(t)/dt$ and its median are shown in Fig. 16(a). And then the sign of $median_2(t)$ after smoothing is shown in Fig. 16(b) in red, which is opposite to the direction of target displacement and is used to identify the target direction. Correct transitions are shown in Fig. 16(b) in blue.

In the optical feedback regime with $0 < C < 0.2$, the SM fringes are almost sinusoidal showing non-symmetrical shape [23]. Existing three transitions detection methods, fix threshold transition detection algorithm [24], adaptive transition detection algorithm [23] and duty cycle algorithm [25], cannot be used in this case. However, the change of C is very common in speckle affected SM signal. As shown in Fig. 15(a), the range of C is from 0.086 to 1.215, which means that the SM feedback regimes varying from very weak to moderate feedback. However transitions are correctly detected by the proposed algorithm, even for

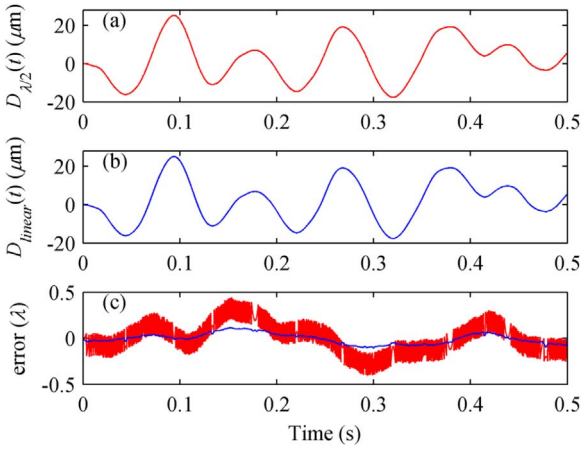

Fig. 17. Displacement reconstructed results for an aleatory displacement: (a) displacement reconstructed by fringe counting $D_{\lambda/2}(t)$, (b) displacement reconstructed by the linearization fringe counting method $D_{linear}(t)$, and (c) error of $D_{\lambda/2}(t)$ (in red) and $D_{linear}(t)$ (in blue). (For interpretation of the references to color in this figure legend, the reader is referred to the web version of this article.)

the segments with $C < 0.2$. It is noted that the proposed method is able to provide a unified algorithm to discriminate the direction of a remote target movement for lasers subjected to different optical feedback regime.

After correct detection of transitions, displacements reconstructed by fringe counting and the linearization fringe counting method are shown in Fig. 17(a) and (b), and the corresponding errors are shown in Fig. 17(c) in red and in blue, respectively. The maximum error by the linearization fringe counting method is less than $\lambda/10$.

5. Experimental validation

The proposed three envelope extraction transition detection algorithm has been tested experimentally. The experimental setup is shown in Fig. 18. A low-cost commercial LD (QL65D5SA, QSI) is used for the SM sensor. Targets are fixed on a high-precision piezoelectric transducer (PZT, PI, P517.3CD). The proprietary capacitive sensor of the PZT measures position with a resolution of 1 nm, and the results are used as the reference measurement of the target displacement. A variable attenuator (VA) is used to adjust the fraction of light back-reflected into the LD's optical cavity. The SM signal monitored by the photodiode (PD) in the LD package is sent through a trans-impedance amplifier, digitized with a data acquisition module (NI, USB6251), and finally processed in a computer.

Fig. 19(b) presents a SM signal of a triangular displacement of 41 μm p-p. The speckle-induced modulation of this signal is about 10.4. As shown in Fig. 19(c), the SM fringes are almost sinusoidal with little distorted, therefore it is hard to identify the direction of target from SM signal directly. By using the proposed technique, a normalized

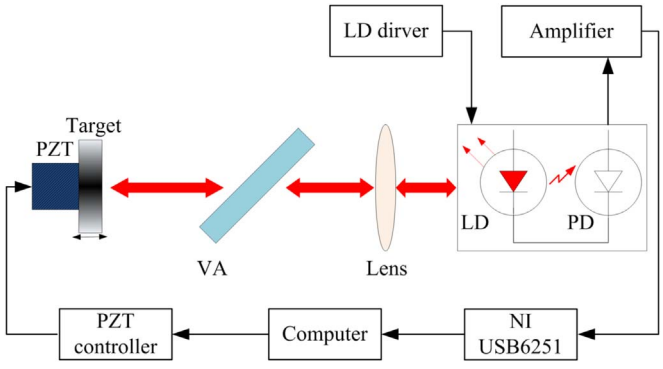

Fig. 18. Experimental setup.

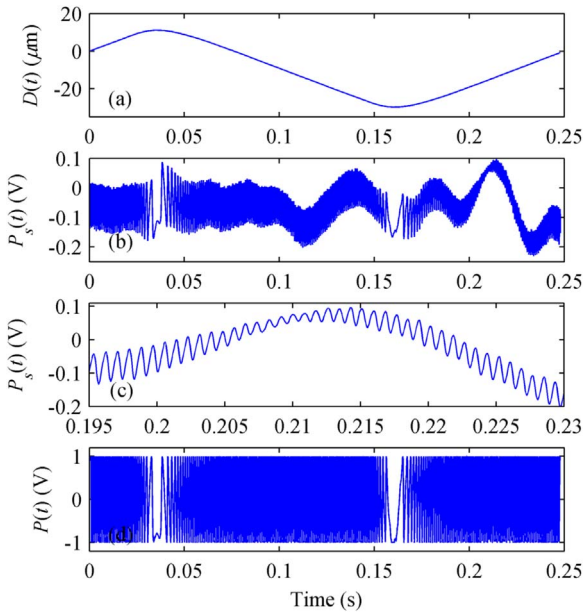

Fig. 19. Waveform processing results: (a) the reference displacement, (b) $P_s(t)$, (c) zoom on the deeply modulated fringes and (d) $P(t)$.

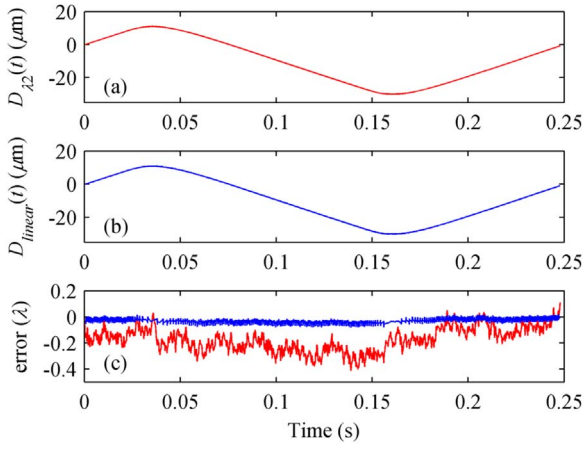

Fig. 20. Displacement reconstructed results for a triangular displacement: (a) $D_{\lambda/2}(t)$, (b) $D_{linear}(t)$ and (c) error of $D_{\lambda/2}(t)$ (in red) and $D_{linear}(t)$ (in blue). (For interpretation of the references to color in this figure legend, the reader is referred to the web version of this article.)

and zero-crossing SM signal $P(t)$ is obtained (Fig. 19(d)), and reconstructed displacements $D_{\lambda/2}(t)$ and $D_{linear}(t)$ are shown in Fig. 20(a) and (b), respectively. Errors compared with the reference displacement (Fig. 19(a)) are shown in Fig. 20(c). The maximum error of $D_{\lambda/2}(t)$ is about 268 nm (~0.4λ), which means that every SM fringe was correctly detected. And the maximum error of $D_{linear}(t)$ is about 53 nm (~0.08λ).

Fig. 21(a) presents a SM signal with a gradual variation in C value by varying the attenuation of VA. By using the proposed method, it has been correctly normalized (Fig. 21(b)) and all transitions are detected. $D_{\lambda/2}(t)$ thus reconstructed was then compared with the reference displacement (Fig. 21(c)). The different between these two signals is shown in Fig. 21(d). The maximum error is 269 nm (~0.4λ) for sinusoidal displacement amplitude of 1.47 μm.

For the large displacement, Fig. 22(a) presents an experimental SM signal with a target displacement of 0.425 mm. The distance between sensor and target is about 100 mm. By using the three envelope extraction transition detection algorithm, the speckle affected SM signal is processed to recover the target displacement (Fig. 22(c)). Fig. 22(d) shows that the maximum error is about 300 nm (0.46λ). It is

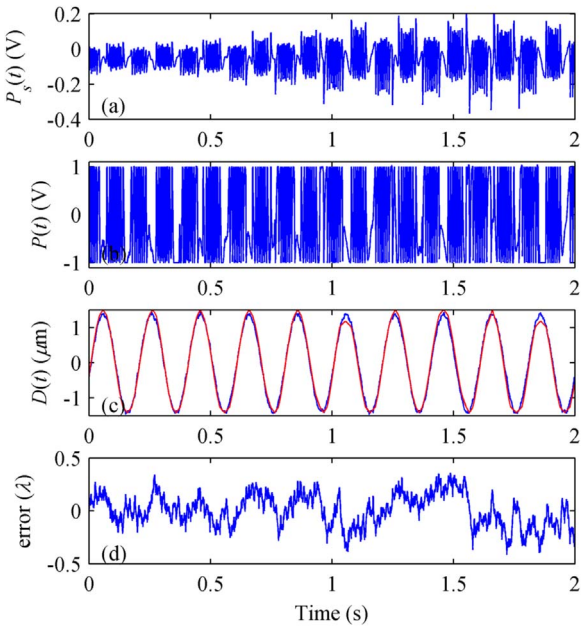

Fig. 21. Displacement reconstructed results for a sinusoidal displacement: (a) $P_s(t)$, (b) $P(t)$, (c) $D_{\lambda/2}(t)$ (in red) and reference displacement (in blue) and (d) error. (For interpretation of the references to color in this figure legend, the reader is referred to the web version of this article.)

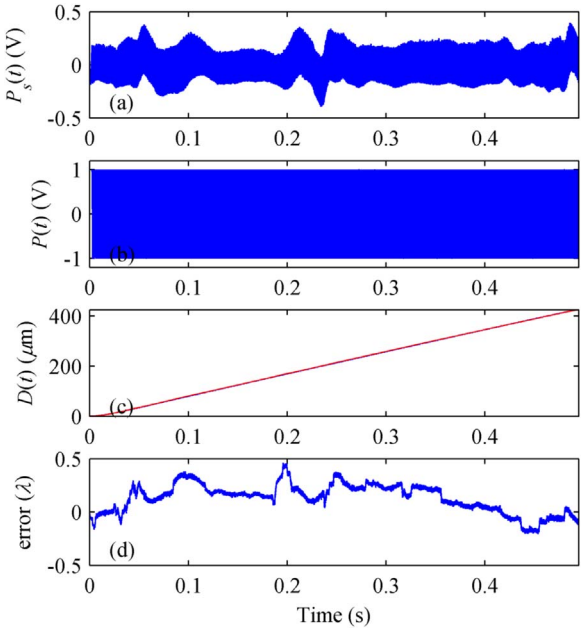

Fig. 22. Displacement reconstructed results for a displacement of 0.425 mm: (a) $P_s(t)$, (b) $P(t)$, (c) $D_{\lambda/2}(t)$ (in red) and reference displacement (in blue) and (d) error. (For interpretation of the references to color in this figure legend, the reader is referred to the web version of this article.)

shown that three envelope extraction transition detection algorithm is able to correctly recover large displacement while SM fringes affected by speckle.

6. Conclusions

In this paper, a simple and effective algorithm has been proposed to improve displacement measurements for SM signals affected by speckle. The proposed three envelope extraction transition detection algorithm is the ability to extract and process SM signals with variable fringe amplitude and different optical feedback regime. It is also able to

discriminate the direction of the target movement by only extracting the sign of the median value from the differential SM signal, even for $0 < C < 0.2$, when the shape of the signal are almost sinusoidal. Experimental results showed that the proposed algorithm has provided a measurement precision of 53 nm for SM signal with the depth of speckle-induced modulation of 10.4. Displacements within a range of 10^{-6} m to 10^{-3} m have thus been recovered from speckle modulated SM signals while avoiding additional optical/electro-mechanical component, strict sampling number determination, and maintaining low the global system cost.

Acknowledgments

The work is financially supported by National Natural Science Foundation of China (11404283), National Natural Science Foundation of Guangdong Province, China (2014A030307028), Program of Young Creative Talents in Universities of Guangdong Province, China (2015KQNCX093), Science and Technology Program of Guangdong, China (2016A040403124), Science and Technology Program of Zhanjiang, China (2013B01138), and Lingnan Normal University Natural Science Foundation (L1204). The authors acknowledge David Bergström of the Luleå University of Technology for providing the rough surface generation code. The authors would like to thank Prof. Jiwen Cui and Yuhang Wang (Center of Ultra-Precision Optoelectronic Instrument, Harbin Institute of Technology) for the help in experiment.

References

[1] J. Perchoux, A. Quotb, R. Atashkhooei, F.J. Azcona, E.E. Ramírez-Miquet, O. Bernal, A. Jha, A. Luna-Arriaga, C. Yanez, J. Caum, Current developments on optical feedback interferometry as an all-optical sensor for biomedical applications, Sensors 16 (2016) 694.
[2] T. Taimre, M. Nikolić, K. Bertling, Y.L. Lim, T. Bosch, A.D. Rakić, Laser feedback interferometry: a tutorial on the self-mixing effect for coherent sensing, Adv. Opt. Photonics 7 (2015) 570–631.
[3] S. Donati, Developing self-mixing interferometry for instrumentation and measurements, Laser Photonics Rev. 6 (2012) 393–417.
[4] W.M. Wang, W.J.O. Boyle, K.T.V. Grattan, A.W. Palmer, Self-mixing interference in a diode laser: experimental observations and theoretical analysis, Appl. Opt. 32 (1993) 1551–1558.
[5] S. Donati, G. Giuliani, S. Merlo, Laser diode feedback interferometer for measurement of displacements without ambiguity, IEEE J. Quantum Elect. 31 (1995) 113–119.
[6] M. Wang, G. Lai, Displacement measurement based on Fourier transform method with external laser cavity modulation, Rev. Sci. Instrum. 72 (2001) 3440–3445.
[7] O.D. Bernal, U. Zabit, T. Bosch, Study of laser feedback phase under self-mixing leading to improved phase unwrapping for vibration sensing, IEEE Sens. J. 13 (2013) 4962–4971.
[8] A.L. Arriaga, F. Bony, T. Bosch, Speckle-insensitive fringe detection method based on Hilbert transform for self-mixing interferometry, Appl. Opt. 53 (2014) 6954–6962.
[9] Y. Tao, M. Wang, W. Xia, Semiconductor laser self-mixing micro-vibration measuring technology based on Hilbert transform, Opt. Commun. 368 (2016) 12–19.
[10] J. Chen, H. Zhu, W. Xia, D. Guo, H. Hao, M. Wang, Synthetic-wavelength self-mixing interferometry for displacement measurement, Opt. Commun. 368 (2016) 73–80.
[11] S. Donati, G. Martini, T. Tambosso, Speckle pattern errors in self-mixing interferometry, IEEE J. Quantum Elect. 49 (2013) 798–806.
[12] M. Norgia, S. Donati, D. D'Alessandro, Interferometric measurements of displacement on a diffusing target by a speckle tracking technique, IEEE J. Quantum Elect. 37 (2001) 800–806.
[13] G. Giuliani, S. Bozzi-Pietra, S. Donati, Self-mixing laser diode vibrometer, Meas. Sci. Technol. 14 (2003) 24–32.
[14] M. Norgia, S. Donati, A displacement-measuring instrument utilizing self-mixing interferometry, IEEE Trans. Instrum. Meas. 52 (2003) 1765–1770.
[15] R. Atashkhooei, S. Royo, F.J. Azcona, Dealing with speckle effects in self-mixing interferometry measurements, IEEE Sens. J. 13 (2013) 1641–1647.
[16] A. Jha, F.J. Azcona, C. Yañez, S. Royo, Extraction of vibration parameters from optical feedback interferometry signals using wavelets, Appl. Opt. 54 (2015) 10106–10113.
[17] U. Zabit, O.D. Bernal, T. Bosch, Self-mixing laser sensor for large displacements: Signal recovery in the presence of speckle, IEEE Sens. J. 13 (2013) 824–831.
[18] P.J. De Groot, G.M. Gallatin, S.H. Macomber, Ranging and velocimetry signal generation in a backscatter-modulated laser diode, Appl. Opt. 27 (1988) 4475–4480.
[19] M. Wang, M. Lu, H. Hao, J. Zhou, Statistics of the self-mixing speckle interference in a laser diode and its application to the measurement of flow velocity, Opt. Commun. 260 (2006) 242–247.
[20] D.M. Kane, K.A. Shore, Unlocking Dynamical Diversity: Optical Feedback Effects On Semiconductor Lasers, fourth ed., John Wiley & Sons Inc., Chichester, UK, 2005.
[21] N. Garcia, E. Stoll, Monte Carlo calculation for electromagnetic-wave scattering from random rough surfaces, Phys. Rev. Lett. 52 (1984) 1798–1801.
[22] D. Bergström, Rough surface generation & analysis, ⟨http://www.mysimlabs.com/surface_generation.html⟩, 2012.
[23] U. Zabit, T. Bosch, F. Bony, Adaptive transition detection algorithm for a self-mixing displacement sensor, IEEE Sens. J. 9 (2009) 1879–1886.
[24] C. Bes, G. Plantier, T. Bosch, Displacement measurements using a self-mixing laser diode under moderate feedback, IEEE Trans. Instrum. Meas. 55 (2006) 1101–1105.
[25] A. Magnani, A. Pesatori, M. Norgia, Self-mixing vibrometer with real-time digital signal elaboration, Appl. Opt. 51 (2012) 5318–5325.